Experimental study and modeling of the behavior of partially saturated asphalt concrete under freezing condition

van Thang Vu, Olivier Chupin, Jean Michel Piau, Ferhat Hammoum, Stéphane Bouron

Experimental study and modeling of the behavior of partially saturated asphalt concrete under freezing condition

Van Thang VU, Olivier CHUPIN, Jean-Michel PIAU, Ferhat HAMMOUM, Stéphane BOURON

IFSTTAR, MAST, F-44344 Bouguenais, France

ABSTRACT

Asphalt pavement damaging characterized by series of potholes was recently observed in France and Northern Europe. This type of pavement distress surprisingly occurred in short time laps over large distances during winters and after rainfalls had taken place. Based on these observations, a specific mechanism is suspected to be responsible for such disorders. This mechanism is believed to be related to the behavior under freezing conditions of asphalt concrete (AC) partially saturated with water, which is the focus of the present research. To investigate this behavior two types of experimental test are carried out in the laboratory. One test is performed under free stress condition while the other test is subjected to restrained strain. The experimental results from these two tests show the development of swelling strain and induced stress in the saturated asphalt specimens, respectively. These two effects are attributed to the phase change of pore water from liquid to solid. A constitutive law taking into account viscoelasticity of AC, thermal expansion and swelling induced by frost is elaborated. This law is implemented in a numerical program and validated against the experimental results.

Keywords: saturated asphalt concrete, freezing, swelling, viscoelasticity, constitutive law.

Construction and Building Materials, 163 (2018), Elsevier, DOI: 10.1016/j.conbuildmat.2017.12.070

1. INTRODUCTION

This research was motivated by field feedbacks showing the apparition of series of potholes taking place in some asphalt pavements in France and other Northern Europe countries. Such degradation occurred almost simultaneously (typically in half a day) over some important part of road sections and under particular weather circumstances combining cold temperatures and rainfall events. Early investigations of these disorders [1][2] have pointed out that a specific mechanism could be at the origin of the problem and that this mechanism was likely related to the mechanical behavior of asphalt concrete (AC) partially saturated with water when subjected to freezing. Traffic and initial damage might represent propitious or aggravating factors to this deterioration mechanism.

The mechanical response of partially saturated AC specimens undergoing freezing then started to be studied in the laboratory [3][4]. Experimental tests were performed at the timescale of one (or a few) frost/thaw cycle(s) focusing on the strain evolution during freezing. Results from these studies show that large swelling strain develops in the AC sample during cooling starting at the time at which temperature in the sample reaches some negative value. This swelling strain is attributed to freezing of the pore water occluded in the AC specimen.

In this paper, we present additional tests performed on saturated AC to quantify the level of strain but also of stress that can originate from freezing of pore water. The objective is then to use these tests to elaborate a constitutive law dedicated to saturated AC. Two tests are considered. One is run considering traction free boundary condition that let the sample deform freely. The other test is performed under restrained strain and makes thermal stress occur in the sample. The tests performed clearly show the impact of the pore water phase change on the experimental data.

It is only recently and following feedbacks from the field that the combined effects of moisture and frost is considered as possibly leading to a frank mechanism of pavement structure deterioration, which often results from fatigue process. This mechanism is not well understood yet and for this reason is investigated in the present work.

Note that in the past, moisture susceptibility and moisture damage of AC was studied putting into evidence its impact on the long term on stripping, raveling, shelling and hydraulic scour [5][6][7][8]. On the other hand, the impact of frost on pavements was also studied in the laboratory but rather from the sight of the long-term effect of repeated cycles [9][10]. Interestingly, the results from this research shows that the internal structure of AC is modified according to the number of cycles applied, resulting in an increase of void ratio and permeability [11][12] and a decrease of the AC stiffness [13]. All these effects can contribute to weaken AC pavements but cannot explain the sudden and simultaneous onset of potholes.

This paper is divided into three main sections. First we present the experimental testing of saturated AC materials. Based on the test results, the development of a constitutive law as well as its implementation in a numerical program is presented in a second part. Finally, this law is validated against experimental data.

2. EXPERIMENTAL TESTING

Two tests are considered in this section to investigate the behavior of partially saturated AC under freezing. The first test performed according to traction free boundary condition is denoted CTFS which is the acronym for Cooling Test in Free Stress condition. This test is used to evaluate swelling strain that develops in saturated AC under freezing condition. The associated dual variable is the freezing-induced stress which is quantified by means of TSRST which stands for Thermal Stress Restrained of Specimen Test. AC samples are subject to restrained strain during this test.

In this section, the AC materials used in the present study and the experimental procedures applicable to each tests are detailed prior to the experimental results are commented.

Material properties and preparation of the AC specimens

The asphalt mixture used in this study is designed according to the French formulation method [14] and is denoted BBSG with a nominal aggregate size of 0/14mm. Its gradation curve is shown in figure 1. A bitumen classified 35/50 with a content of 4.45 ppc was used.

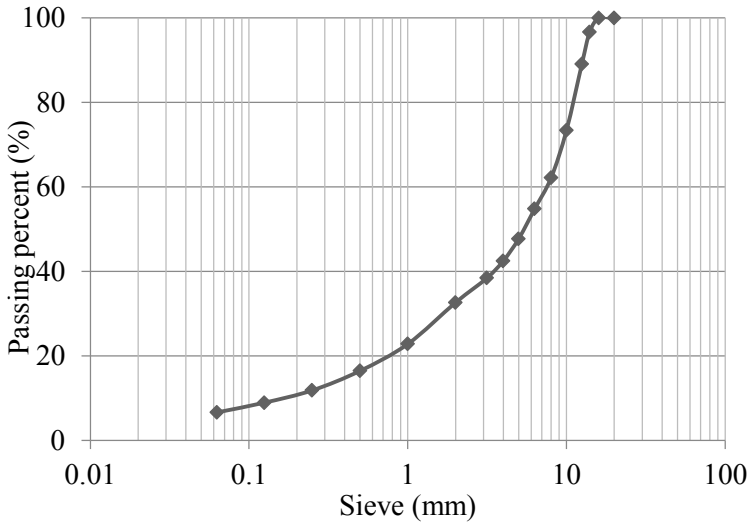

Figure 1**:** Grading curve of the aggregates

The test specimens used in CFTS and TSRST are cored in slabs of BBSG 0/14 that were compacted using the plate-compactor machine. Two series of cylindrical specimens are designed to comply with the geometry required by each test. Dimensions of the specimens used in CFTS are 80 mm in diameter (Ø80) and 120 mm in height. All these specimens (6 in total) are cored vertically from the same slab. For use in TSRST, 8 cylindrical specimens of diameter 50 mm (Ø50) and of height 160 mm are core-drilled horizontally according to the European standard NF EN 12967-46. Porosity of every specimen is checked by means of the X-ray method [15], which is performed for both dry and partially saturated AC samples. Saturation of an AC specimen is obtained considering the following process: (i) a negative pressure of -86kPa is applied during one hour to the initially dry specimen placed in a tank,

(ii) water is slowly added until full immersion of the specimen then maintaining the negative pressure during three hours. For all the specimens tested, the degree of saturation determined by weight measurements is found to be around 60% (Table 1).

Type of test	Number of specimens tested	Specimen dimensions (mm)	Average porosity (%)	Average degree of saturation (%)	Test details
CTFS	6	Ø80 × 120	6.2	63	All specimens are tested successively under dry and wet conditions
TSRST	8	Ø50 × 160	6.5	60	3 specimens are tested under dry conditions and 5 under wet conditions

Table 1: Summary of the experimental campaign carried out

Experimental procedures

The experimental procedures specific to the CFTS and TSRST tests are described in this section. In particular, instrumentation of the samples is focused on as well as the evolution of temperature imposed to the samples.

Cooling test in free stress conditions (CTFS)

In this test, the cylindrical AC specimens (Ø80 × 120 mm) are equipped with two strain gages and a temperature sensor glued on surface of the specimen at mid-height (Fig. 2a). One of the strain gages is positioned vertically and thus measures the axial strain while the other placed horizontally measures strain in the (ortho-) radial direction. Both gages are protected against external temperature and moisture by a silicone coating.

The instrumented specimens are tested imposing traction-free boundary condition all over their outer surface within a climatic chamber. The controlled temperature of the climatic chamber is varied from 10 °C to -10 °C as shown in figure 2b. The specimens are tested first under dry conditions and then after partial saturation performed as explained before. The axial and radial strain evolutions are recorded during cooling of the AC samples which are free to deform given the mechanical boundary conditions.

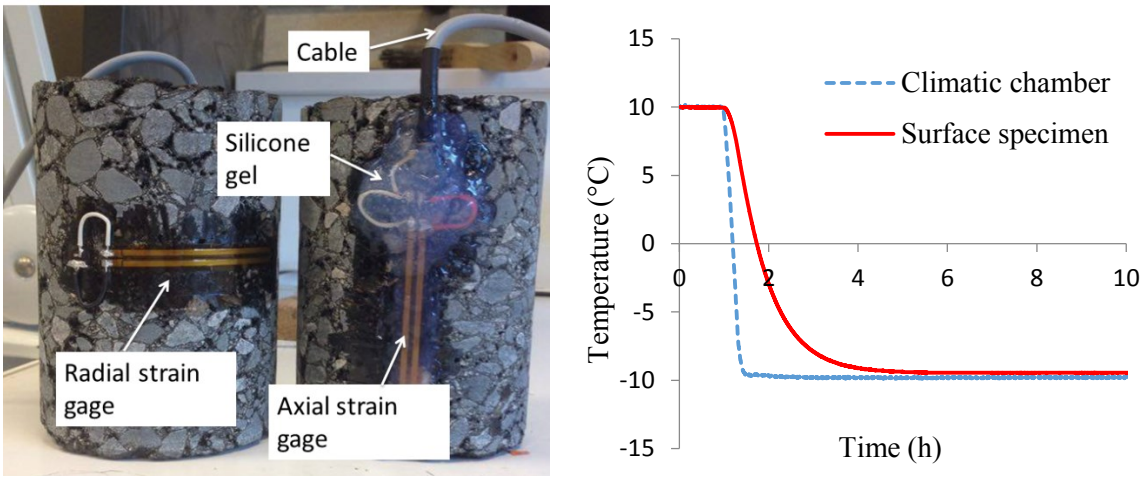

(a) (b)

Figure 2: (a) Picture of the instrumented AC specimen. (b) Evolution of the controlled temperature of the climatic chamber and of the temperature measured at the surface of a dry AC specimen during CTFS testing.

Since strain gages are sensitive to temperature, their raw measurement must be corrected to obtain the correct value of strain under variable temperature. In this study, the correction is done based on the measurement of a particular gage glued on an invar rod also placed in the climatic chamber and thus subjected to the same controlled temperature as the AC samples. Invar is an alloy having a very small coefficient of thermal expansion ($\alpha_{Invar} \approx 0.03\ \mu m/m/°C$).

The strain recorded on the AC sample can be decomposed into the following parts:

$$\varepsilon_{AC}^{measure}(t) = \varepsilon_{AC}^{true}(t) + \varepsilon_{gage}^{err}(t) \quad (1)$$

And that recorded on the Invar rod as follows:

$$\varepsilon_{Invar}^{measure}(t) = \varepsilon_{Invar}^{true}(t) + \varepsilon_{gage}^{err}(t) \quad (2)$$

Quantity $\varepsilon_{gage}^{err}(t)$ reflects the measurement bias brought by the gage sensitivity to temperature. However, considering that α_{Invar} is negligible then $\varepsilon_{Invar}^{true}(t) = \alpha_{Invar}\,\Delta\theta \sim 0$ and the actual (corrected) strain of AC samples is given by:

$$\varepsilon_{AC}^{true}(t) = \varepsilon_{AC}^{measure}(t) - \varepsilon_{Invar}^{measure}(t) \quad (3)$$

Thermal stress restrained specimen test (TSRST)

This test is adapted from the European standard NF EN 12967-46 (TSRST). The cylindrical specimens ($\emptyset 50 \times 160\ mm$) tested are clamped between two press pistons and placed into a climatic chamber, the controlled temperature of which is decreased at the rate of 10 °C/h (Fig 3b). The length of the specimen is maintained constant during the test by acting on the force imposed between the two pistons. The value of stress in the AC specimen is inferred from this force that ensures a zero longitudinal strain during testing. This is controlled through the corrected measurement (as described in the previous section) of a strain gage glued to the lateral surface of the AC specimens.

The TSRST campaign carried out in this study involves eight AC specimens among which three are tested under dry conditions and five after saturation.

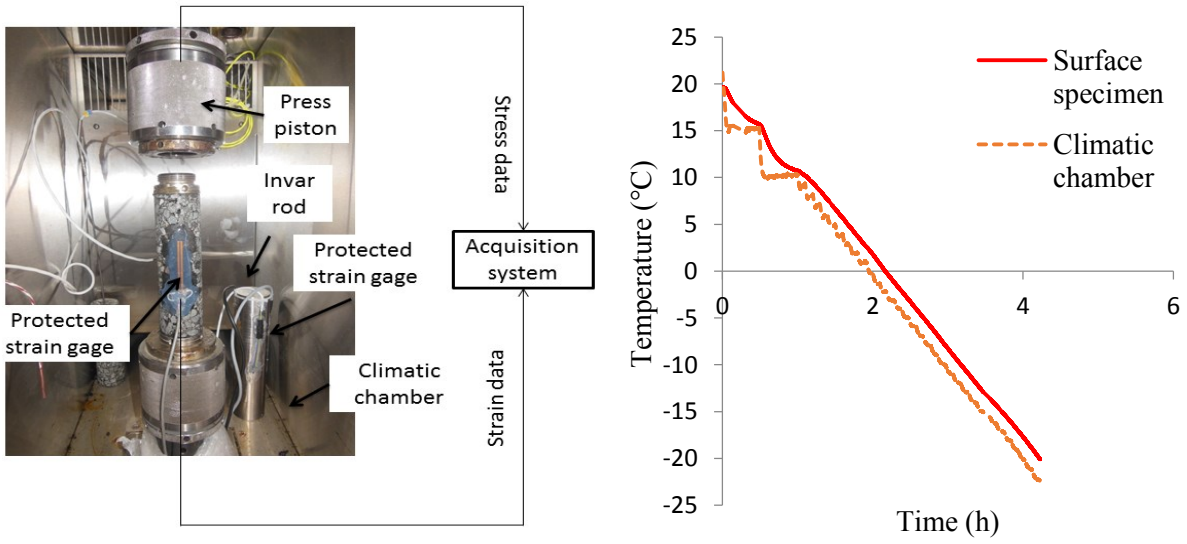

(a) (b)

Figure 3: (a) Experimental set-up used in TSRST testing. (b) Evolution of the controlled temperature of the climatic chamber and of the temperature measured by a sensor glued at the surface of an AC specimen.

Note that to avoid variability effect from one sample to another in the comparison between the two tests considered in this paper, some saturated AC samples are utilized for both CTFS testing and then TSRST testing after the saturation has been set back to the initial level.

Results and discussions

Effect of water phase change on the measured strain evolution during CTFS testing

Some typical experimental results from CTFS testing are presented below showing the corrected strain evolution with respect to time. In particular, figure 4 displays the comparison between the radial and the axial strain obtained for the same AC sample tested under dry and wet conditions. The AC specimen under consideration has a porosity of 7.7% ($n = 7.7\%$) and a degree of saturation equal to 65% ($S_r = 65\%$).

As expected during cooling, the radial and the axial strain curves show an isotropic thermal contraction under dry condition. In this case, the change in strain for a temperature variation of -20 °C ($\Delta\theta = -20\,°C$) is about -500 $\mu strain$ reflecting a coefficient of thermal expansion equal to 25 $\mu m/m/°C$, which is typical of AC materials.

Concerning the saturated specimen, the evolution of the axial and the radial strain is similar at the beginning to that obtained under dry condition. However, it exhibits for a while afterwards a "chaotic" phase composed of several peaks oriented opposite to the strain direction observed until that moment during cooling. Once this phase is over, the strain evolution becomes smooth again till the end of the test and is homothetic to the temperature curve whose decrease is ending at this time to eventually reach a plateau. During the "chaotic" phase, the evolution of the axial strain is not exactly similar to that of the radial strain but the two curves are superimposed again during the last part of the test.

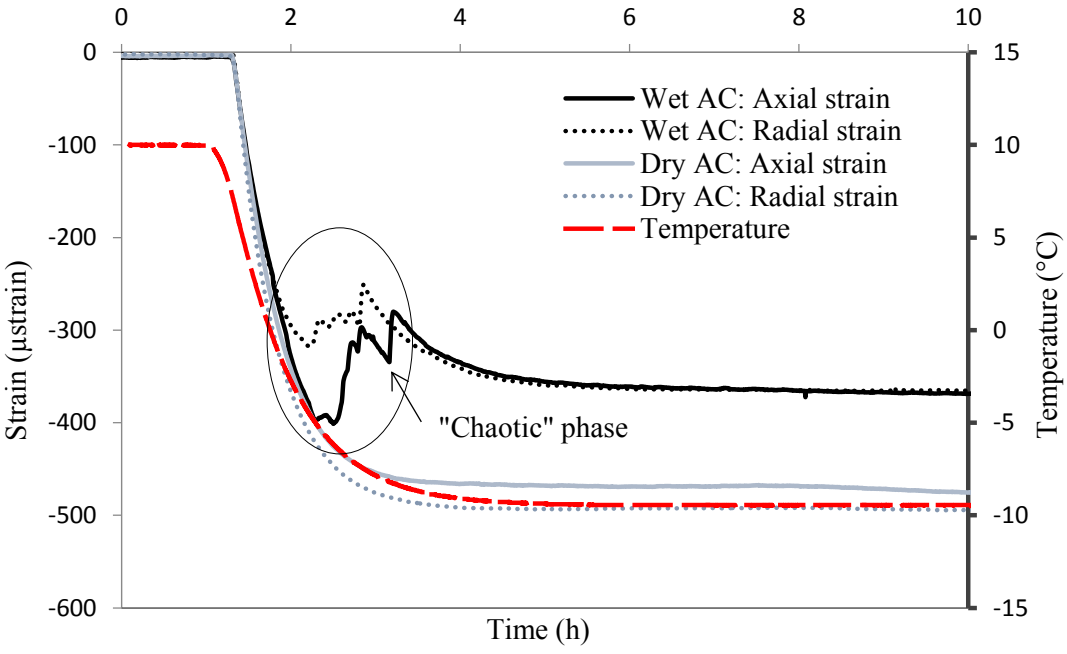

Figure 4: Corrected measurements of the axial and the radial strain recorded for an AC sample tested under dry and wet conditions ($n = 7.7\%$ and $S_r = 65\%$) and temperature evolution measured on the outer surface of the dry specimen during CTFS testing.

179 The comparison between the strain plateaus obtained for the dry and the wet specimens at the
180 end of the test at a temperature of -10 °C shows a positive difference (swelling) of about
181 130 µstrain and 110 µstrain in the radial and the axial direction, respectively. This difference
182 clearly results from the "chaotic phase" which undoubtedly can be associated to the water
183 phase change from liquid to ice within the whole sample. Indeed solidification is known to
184 induce an increase of 9% in volume in the case of free water. For the six tests of the CTFS
185 campaign, the swelling ("chaotic") phase starts as the external temperature is below -2 °C
186 instead of 0 °C probably due to several physical phenomena taking place in the AC samples.
187 These phenomena can be related to capillary forces, stagnancy of pore water and super
188 cooling effect, the chemical change of pore water at contact with the aggregates, etc.
189 Figure 5 shows a summary of the results obtained in this campaign. As displayed in figure 5a
190 on the left, the coefficients of thermal expansion calculated for the dry specimens in the axial
191 and the radial directions can be considered similar; the relative difference between them is
192 lower than 3%. On the other hand, figure 5b shows that the relative difference in terms of
193 swelling strain obtained in the two directions is also very small and of the order of 6%.
194 Consequently, the behavior of the AC specimens (dry or saturated) can be assumed as
195 isotropic.

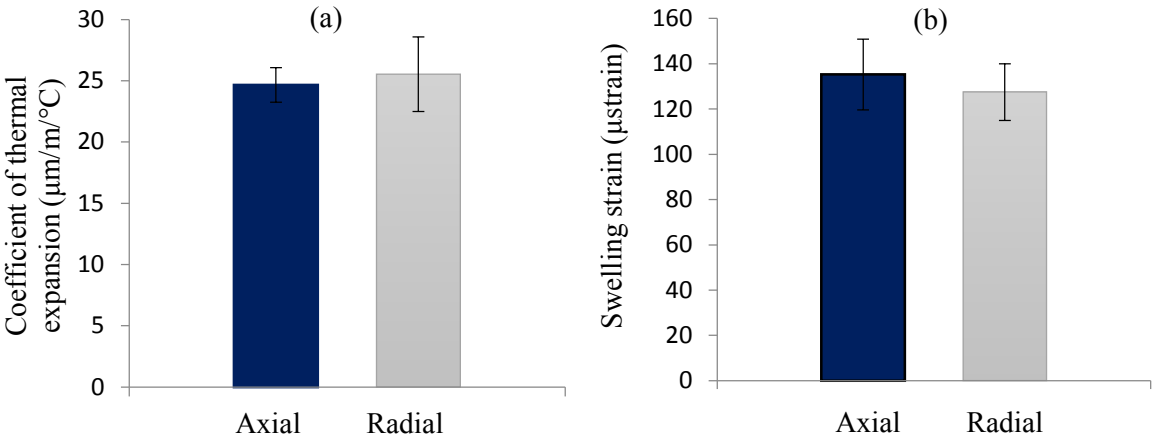

Figure 5: Comparison between the corrected measurements recorded in the axial and the radial directions: (a) Coefficients of thermal expansion for the dry specimens. (b) Swelling strains in the case of saturated specimens. (Error bars show the standard deviation of the measurements performed on 6 samples).

Effect of water phase change on the measured stress evolution during TSRST testing

Representative results from TSRST testing are shown in figure 6a which displays the stress evolution obtained for dry and wet specimens when temperature is decreased from 20 °C to -30 °C. The dry and the saturated AC samples have a porosity of 5.9% and 5.1%, respectively. The saturated sample was first subjected to CTFS testing and then to TSRST testing once saturation has been refilled to the initial level of 60%. The swelling strain for the saturated AC specimen is inferred from the difference between the final plateaus resulting from CTFS testing (Fig. 6b); a value of 150 µstrain is obtained (axial direction).

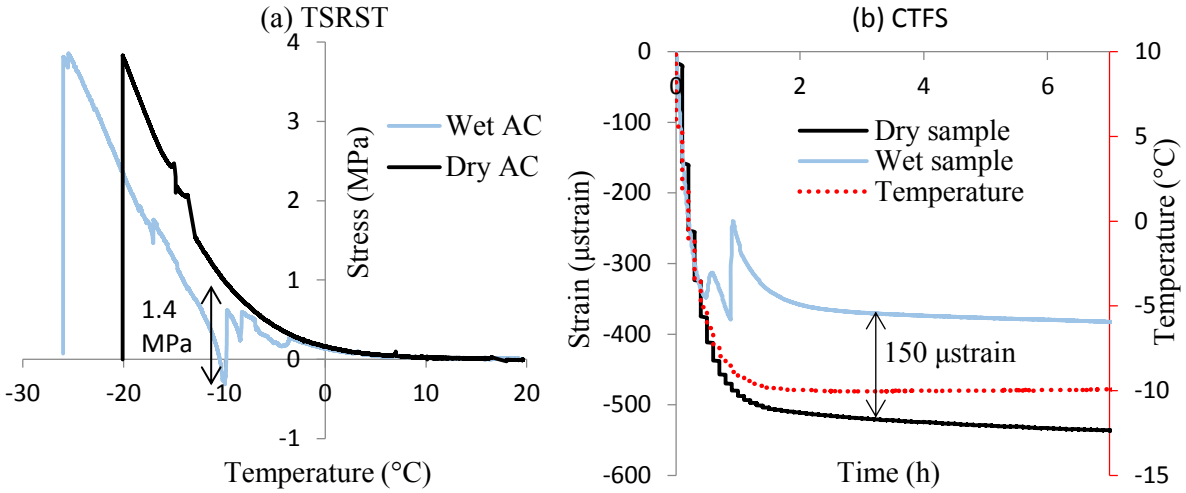

Figure 6: Comparison between the mechanical responses in terms of stress and strain obtained for the dry and wet AC samples: (a) TSRST, (b) CTFS

Concerning stress evolution, the dry AC sample exhibits the characteristic response of asphalt concrete materials tested according to the TSRST protocol (Fig 6a); the axial tensile stress increases as temperature decreases to compensate thermal contraction. Due to hardening of the AC material with temperature (loss of relaxation capability), the tensile stress increases more and more as temperature diminishes. The tests stops brutally at failure of the specimen (*i.e.* 4 MPa at -21 °C), as illustrated by the drop of the stress curve in figure 6a.

At the beginning of the test and as long as temperature is higher than the freezing point of pore water detected at around -5°C, the saturated sample exhibits a quite similar response as the dry sample. For temperature variations from -5 °C to -10 °C, a decrease of the stress magnitude is then observed, even leading to slight compression at -10 °C. Afterward, the stress curve for the wet AC becomes similar again to that of the dry AC, remaining parallel to it but below. Failure of the (partially) saturated specimen is reached for the same stress value as the dry specimen (≈ 4 MPa) but at a lower temperature (-26 °C instead of -21 °C). Basically, the shift between the two curves can be interpreted by a compressive stress of magnitude 1.4 MPa developing in the specimen during the phase change of water into ice. Comparison of the CTFS and the TSRST results for this saturated specimen indicates that the

1.4 MPa “swelling stress” can be considered roughly as the counterbalance effect of the 150×10^{-6} “swelling strain” through a secant modulus of 10,000 MPa during the water phase change.

The trend observed for this particular sample is confirmed by the rest of the TSRST campaign. The average temperature at failure is lower for the saturated than for the dry specimens. The values obtained are -23 ±2.5°C and -20.3 ±0.5°C, respectively (Fig 7). On the other hand, the average critical stress value at material failure seems to be slightly higher for dry than for saturated specimens with values equal to 3.8±0.01 MPa and 3.37±0.4 MPa, respectively (Fig 7).

However, note that the lower temperature obtained at failure for the saturated specimens must not be interpreted as an improvement of mechanical performance of the material in presence of water. TSRST test rather shows that a frost front propagating into saturated AC layers of pavements can develop unexpected internal stress field which effects need to be further investigated.

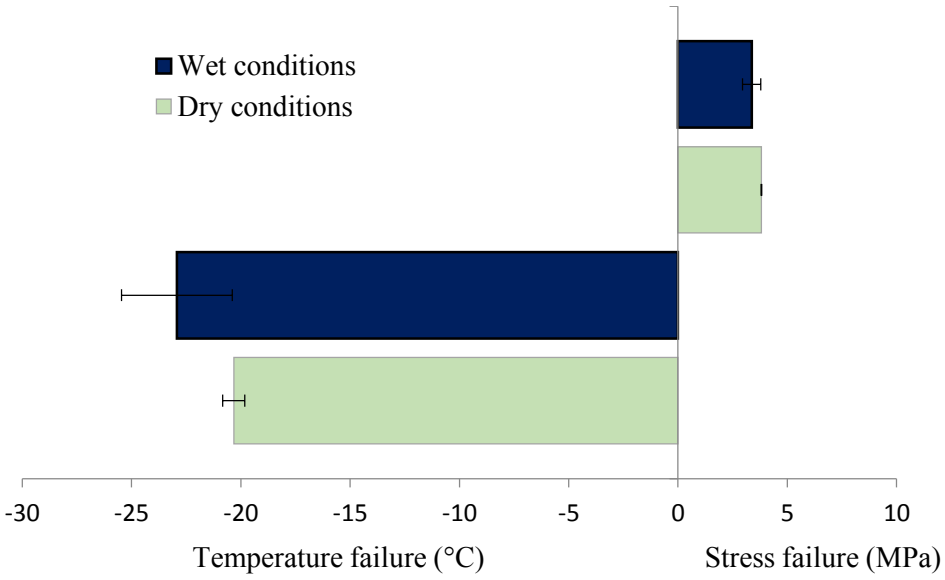

Figure 7: Comparison between the dry and the saturated AC specimens in terms of temperature and critical stress obtained at failure (averaged over all the samples of the TSRST campaign and error bars show the standard deviation of the measurements performed on 3 dry and 5 saturated samples).

Effect of water phase change on the creep properties

The impact of the phase change of pore water into ice on the creep function was studied in [16] on the basis of complex modulus test campaigns performed on the same AC sample in dry and saturated conditions. For temperatures above the freezing point of pore water no difference is observed between these two conditions, whereas ice formation is found to increase the stiffness of saturated AC specimens. However, the increase is less than 10 % and is not considered in the following.

3. CONSTITUTIVE MODEL DEDICATED TO THE BEHAVIOR OF SATURATED AC EXPOSED TO FREEZING

The experimental results presented earlier in this paper are used here to develop a constitutive law for the modeling of the thermo-mechanical behavior of partially saturated AC materials exposed to freezing. As well known, bituminous mixes are thermo-sensitive materials exhibiting viscoelastic properties which are accurately captured by the Huet model [17]. Consequently, the developed law is based on this model and extends its scope to taking into account variable temperature condition, thermal expansion and swelling effects due to phase change of pore water.

The development of the constitutive law is presented step-by-step in this section, going from the unidimensional behavior of AC under isothermal condition to the full tridimensional expression including all the aforementioned physical phenomena, especially frost effects. The developed constitutive law is then discretized in time and implemented in a numerical program. Finally this law is used to model the CTFS and the TSRST tests and is validated against the experimental data.

The Huet model under isothermal condition

Rheological model and strain as a convolution integral (1D)

The Huet model is a viscoelastic model composed of a linear elastic spring of modulus E_∞ connected in series with two parabolic dashpots of exponent k and h (Fig 8). The creep function for this model depends on time, t, and temperature, θ, and reads:

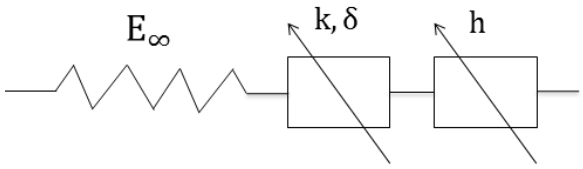

Figure 8: The Huet rheological model.

$$J_H(t,\theta) = J_{h,k}\left(\frac{t}{a(\theta)}\right) \tag{4}$$

With

$$J_{h,k}(u) = \frac{1}{E_\infty}\left(1 + \frac{u^h}{\Gamma(h+1)} + \delta\frac{u^k}{\Gamma(k+1)}\right) \tag{5}$$

in which $\Gamma(\cdot)$ stands for the gamma function and δ is a weight parameter associated to the dashpot of exponent k.

The creep function is written with respect to the single scalar variable $\frac{t}{a(\theta)}$ by virtue of the time-temperature equivalence principle applying for asphalt materials. $a(\theta)$ denotes the time-temperature shift factor, which in this work is expressed as follows:

$$a(\theta) = exp(A_0 + A_1\theta + A_2\theta^2) \tag{6}$$

where A_0, A_1 and A_2 are constant parameters of the model.

The Huet model parameters can be identified using experimental data stemming from complex modulus tests performed in the frequency domain.

The constitutive law is then provided by the mathematical relationship below (of type Stieltjes convolution integral), which expresses the strain response (ε) to the stress history function σ:

$$\varepsilon(t) = J_H(t,\theta) \otimes \dot{\sigma}(t) = \int_{-\infty}^{\infty} J_H(t-\tau,\theta)\,\frac{d}{dt}\sigma(\tau)d\tau \quad (7)$$

Tridimensional strain response in the time domain

For an isotropic material, the above constitutive equation (Eq. 7) can be extended to the tridimensional case by considering the deviatoric and the volumetric components of strain and stress tensors and introducing the creep function for each of them. In this paper, Poisson's ratio is assumed real and constant leading to the following Hooke type constitutive relationship:

$$\boldsymbol{\varepsilon}(t) = J_H(t,\theta) \otimes \left[(1+\nu)\dot{\boldsymbol{\sigma}}(t) - \nu\, tr\left(\dot{\boldsymbol{\sigma}}(t)\right)\boldsymbol{I}\right] = \int_0^t J_H(t-\tau,\theta)\,\frac{d}{dt}\left[(1+\nu)\dot{\boldsymbol{\sigma}}(\tau) - \nu\, tr\left(\dot{\boldsymbol{\sigma}}(\tau)\right)\boldsymbol{I}\right]d\tau \quad (8)$$

where $\boldsymbol{\varepsilon}$, $\boldsymbol{\sigma}$ are tensors of strain and stress, respectively and $\mathbf{I}$ is the unit 3×3 tensor

Constitutive law for asphalt materials under variable temperature condition

Temperature variation has two significant effects to be considered on the behavior of dry asphalt materials: (i) thermal expansion, (ii) change of creep function. Considering the case of saturated AC material, a third effect due to swelling has to be added as shown by the experimental findings presented before.

Model for the case of dry AC material

The thermal expansion is accounted for through the classical relationship:

$$\boldsymbol{\varepsilon}^{th}(\theta) = \alpha\, \Delta\theta\, \boldsymbol{I} \tag{9}$$

in which α is the coefficient of thermal expansion ($\mu m/m/°C$) and $\Delta\theta(t) = \theta(t) - \theta_o$ is the difference between the temperature at time t and that of the reference state denoted θ_o.

On the other hand, the computation of the mechanical strain under variable temperature can be achieved using the concept of "equivalent time" defined by [18]:

$$t_e(t) = \int_0^t \frac{d\tau}{a(\theta(\tau))} \tag{10}$$

This expression can be easily derived for a Kelvin-Voigt model which viscosity is proportional to $a(\theta)$. Using the time t_e instead of t makes it possible to express this model as a Kelvin Voigt constitutive law but with constant viscosity and independently of the temperature. This property extends to the Huet model using the spectral decomposition of its creep function as an infinite series of Kelvin Voigt elements which viscosity depends for all of them upon the same $a(\theta)$ function.

Considering only on the mechanical strain, the Stieltjes integral then writes:

$$\boldsymbol{\varepsilon}(t_e) = \int_0^{t_e} J_{h,k}(t_e - \tau_e)\left[(1+\nu)\frac{\boldsymbol{d\sigma}}{\boldsymbol{dt_e}}(\tau_e) - \nu\, tr\, \frac{\boldsymbol{d\sigma}}{\boldsymbol{dt_e}}(\tau_e)\, \boldsymbol{I}\right] d\tau_e \quad (11)$$

That is, coming back to time *t* and taking also the thermal strain part, the viscoelastic law under variable temperature:

$$\boldsymbol{\varepsilon}(t) = \int_0^{t} J_{h,k}(t_e(t) - t_e(\tau))\,[(1+\nu)\dot{\boldsymbol{\sigma}}(\tau) - \nu\, tr\, \dot{\boldsymbol{\sigma}}(\tau)\, \boldsymbol{I}]d\tau + \boldsymbol{\varepsilon}^{th}\big(\theta(t)\big) \quad (12)$$

Model for the case of partially saturated AC material

In addition to thermal expansion and change in the creep (resp. relaxation) capability and as evidenced by the experimental tests presented in section 2, saturated AC exhibits swelling effects when temperature is varied passing through the freezing point of pore water.

With regards to CTFS test, here we suggest to model the swelling effects by adding a strain component $\boldsymbol{\varepsilon}_f$ to the constitutive law (Eq. 12). This one is assumed isotropic and depending on the difference between the temperature of the material and that of the freezing point of pore water θ_f. As already mentioned, θ_f may depend on several physical phenomena taking place in the porous asphalt and not considered in the model. From the macroscopic point of view of the present approach, θ_f is set according to the temperature at which the behavior of the saturated AC sample departs from that of the dry sample in the experimental tests. Thus, the swelling strain is defined as:

$$\boldsymbol{\varepsilon}_f\big(\theta(t)\big) = \varepsilon_{f0}\frac{1-tanh[m(\theta(t)-\theta_f)]}{2}\,\boldsymbol{I} \quad (13)$$

where m is a parameter that allows us to adjust the temperature range (centered in θ_f) for which most of the swelling deformation occurs (Figure 9). This parameter is used to calibrate the transition of ε_f from zero prior to freezing to ε_{f0} after full completion of the phase change of pore water. Depending on the value of m, this transition can go from quite smooth to sharp.

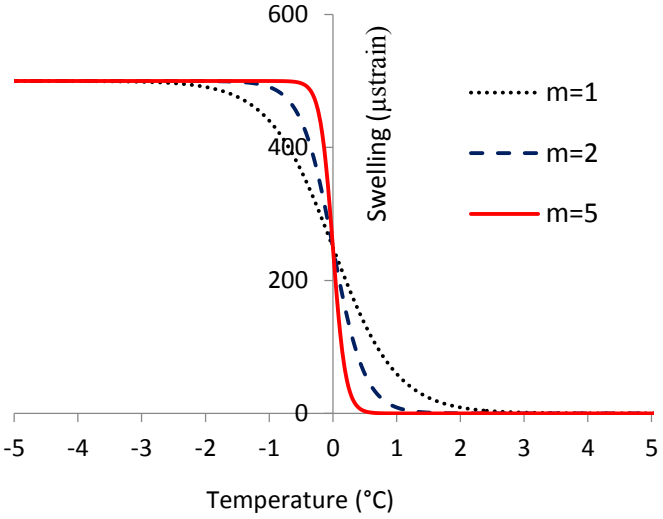

Figure 9: Swelling strain as a function of temperature for different values of parameter m and $\theta_f = 0\,°C$

Finally, the constitutive law developed to represent the thermo-mechanical behavior of AC partially saturated with water can be schematized by the rheological model shown in figure 10. Considering a constant Poisson's ratio, the three dimensional expression of this law (for variable temperature) is given by:

$$\boldsymbol{\varepsilon}(t) = \int_0^t J_{h,k}(t_e(t) - t_e(\tau))\,[(1+\nu)\dot{\boldsymbol{\sigma}}(\tau) - \nu\, tr\,\dot{\boldsymbol{\sigma}}(\tau)\;\boldsymbol{I}]d\tau + \boldsymbol{\varepsilon}^{th}\big(\theta(t)\big) + \boldsymbol{\varepsilon}_f\big(\theta(t)\big) \quad (14)$$

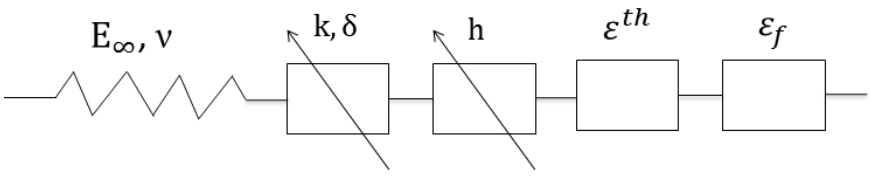

Figure 10: Sketch of the rheological model developed to model saturated AC materials.

365

366 **Time discretization of the three-dimensional constitutive law**

367 As shown by Eq. (14) the developed constitutive law is complex and its use requires
368 numerical computation. In this section, we present the time discretization of this law for
369 isothermal and variable temperature conditions. For both cases, expression of the strain tensor
370 at time t_n for a given stress history function is derived as well as the dual expression of the
371 stress tensor in response to a given strain history function.

372 *Constitutive law in isothermal condition*

373 Under this condition, the θ variable is omitted in the following equations. Using the Euler
374 method and considering the time interval $[t_i, t_{i+1}]$, we approximate the time derivative of the
375 stress tensor in Eq. (12) by the following finite difference: $\dot{\boldsymbol{\sigma}}(\mathrm{t}) \approx \frac{\boldsymbol{\sigma}_{\mathrm{i+1}}-\boldsymbol{\sigma}_{\mathrm{i}}}{\Delta \mathrm{t}}$, where $\Delta t =$
376 $t_{i+1} - t_i$ is the time step assumed constant. At first, we focus on the assessment of $\boldsymbol{\varepsilon}(t_n)$ at
377 the different times $t_0,\ t_1, \ldots, t_i, \ldots\ t_N$ resulting from the following implicit calculation of
378 Eq. (12):

379 $$\boldsymbol{\varepsilon}(t_n) \approx \sum_{i=0}^{n-1} \int_{t_i}^{t_{i+1}} J_H(t_n - \tau) d\tau \frac{(1+\nu)[\boldsymbol{\sigma}_{i+1}-\boldsymbol{\sigma}_i]-\nu\ tr(\boldsymbol{\sigma}_{i+1}-\boldsymbol{\sigma}_i)\,\boldsymbol{I}}{\Delta t} \quad (15)$$

380 Here we assume that at step n all strain and stress quantities $\boldsymbol{\varepsilon}_{\mathrm{i}}$, $\boldsymbol{\sigma}_{\mathrm{i}}$ for $0 \leq i \leq n-1$ have
381 already been computed and are known.
382 The definite integral of the creep function at each time step is computed according to the
383 trapezoidal rule, which for only one interval between t_i and t_{i+1} leads to:

384 $$\boldsymbol{\varepsilon}(t_n) \approx \sum_{i=0}^{n-1} \frac{J_H(t_n-t_{i+1})+J_H(t_n-t_i)}{2} \Delta t \times \frac{(1+\nu)[\boldsymbol{\sigma}_{i+1}-\boldsymbol{\sigma}_i]-\nu\ tr(\boldsymbol{\sigma}_{i+1}-\boldsymbol{\sigma}_i)\,\boldsymbol{I}}{\Delta t} \quad (16)$$

For the sake of simplification, we denote by $\overline{\boldsymbol{\chi}}$ the tensor of all the known values from t_0 to t_{n-1} related to history of the stress tensor. $\overline{\boldsymbol{\chi}}$ is defined by:

$$\overline{\boldsymbol{\chi}} = J_{H_{n,n}}\left[(1+v)\,\boldsymbol{\sigma}(t_{n-1}) - v\,tr\left(\boldsymbol{\sigma}(t_{n-1})\right)\boldsymbol{I}\right] - \sum_{i=0}^{n-2} J_{H_{n,i+1}}\left[\left[(1+v)\boldsymbol{\sigma}(t_{i+1}) - v\,tr\boldsymbol{\sigma}(t_{i+1})\,\boldsymbol{I}\right] - \left[(1+v)\boldsymbol{\sigma}(t_i) - v\,tr\boldsymbol{\sigma}(t_i)\,\boldsymbol{I}\right]\right] \quad (17)$$

in which:

$$J_{H_{n,i+1}} = \frac{J_H(t_n - t_{i+1}) + J_H(t_n - t_i)}{2} \quad (18)$$

Using this notation, Eq. (17) simply reads:

$$\boldsymbol{\varepsilon}(t_n) = J_{H_{n,n}}\left[(1+v)\,\boldsymbol{\sigma}(t_n) - v\,tr\left(\boldsymbol{\sigma}(t_n)\right)\boldsymbol{I}\right] - \overline{\boldsymbol{\chi}} \quad (19)$$

Eq. (19) can be used to compute the response in terms of strain at time t_n to a prescribed stress history function. To obtain the response in terms of stress to an imposed strain history function, Eq. (19) must be reversed. To accomplish this, we first notice from Eq. (19) that:

$$tr\,\boldsymbol{\sigma}(t_n) = \frac{1}{(1-2v)J_{H_{n,n}}}\left[tr\,\boldsymbol{\varepsilon}(t_n) + tr(\overline{\boldsymbol{\chi}})\right] \quad (20)$$

Substituting Eq. (20) into Eq. (19) leads to:

$$\boldsymbol{\sigma}(t_n) = \frac{1}{(1+v)J_{H_{n,n}}}\left[\boldsymbol{\varepsilon}(t_n) + \overline{\boldsymbol{\chi}}\right] + \frac{v}{(1+v)(1-2v)J_{H_{n,n}}}\left[tr\boldsymbol{\varepsilon}(t_n) + tr\overline{\boldsymbol{\chi}}\right]\boldsymbol{I} \quad (21)$$

With:

$$\lambda_n = \frac{v}{(1-2v)(1+v)J_{H_{n,n}}}, \text{ and } \mu_n = \frac{1}{2(1+v)J_{H_{n,n}}} \quad (22)$$

the expression of the stress tensor at the time t_n is finally given by:

$$\boldsymbol{\sigma}(t_n) = 2\mu_n \boldsymbol{\varepsilon}(t_n) + \lambda_n tr\boldsymbol{\varepsilon}(t_n)\boldsymbol{I} + 2\mu_n\, \overline{\boldsymbol{\chi}} + \lambda_n\, tr\overline{\boldsymbol{\chi}}\, \boldsymbol{I} \tag{23}$$

This equation at time t_n is similar to Hooke's law with "initial" stress.

Constitutive law for variable temperature condition

In the case of a partially saturated AC subjected to variable temperature condition the constitutive law is given by Eq (14). Its discretized expression is derived in a similar way as that of the isothermal case adding the concept of equivalent time, thermal expansion and the swelling strain. The discretized form at time t_n reads:

$$\boldsymbol{\varepsilon}(t_n) = \tilde{J}_{H\,n,n}\left[(1+\upsilon)\,\boldsymbol{\sigma}(t_n) - \upsilon\, tr\left(\boldsymbol{\sigma}(t_n)\right)\boldsymbol{I}\right] - \overline{\boldsymbol{\chi}}' + \boldsymbol{\varepsilon}^{th}\left(\theta(t_n)\right) + \boldsymbol{\varepsilon}_{\boldsymbol{f}}(\theta(t_n)) \tag{24}$$

where the quantities

$$\tilde{J}_{H\,n,i+1} = \frac{J_H(t_e(t_n)-t_e(t_{i+1}))+J_H(t_e(t_n)-t_e(t_i))}{2} \tag{25}$$

are now computed considering the equivalent time evaluated as:

$$t_e(t_n) = \int_0^{t_n} \frac{d\tau}{a(\theta(\tau))} = \sum_{i=0}^{n-1} \frac{\Delta t}{2}\left[\frac{1}{a(\theta(t_{i+1}))} + \frac{1}{a(\theta(t_i))}\right] \tag{26}$$

The tensor $\overline{\boldsymbol{\chi}}'$ refers to quantities evaluated for past times (from t_0 to t_{n-1}) and is given by:

$$\overline{\boldsymbol{\chi}}' = \tilde{J}_{H\,n,n}\left[(1+\nu)\,\boldsymbol{\sigma}(t_{n-1}) - \nu\, tr\left(\boldsymbol{\sigma}(t_{n-1})\right)\boldsymbol{I}\right] - \sum_{i=0}^{n-2} \tilde{J}_{H\,n,i+1}\left[\left[(1+\nu)\,\boldsymbol{\sigma}(t_{i+1}) - \nu\, tr\boldsymbol{\sigma}(t_{i+1})\,\boldsymbol{I}\right] - \left[(1+\nu)\,\boldsymbol{\sigma}(t_i) - \nu\, tr\boldsymbol{\sigma}(t_i)\,\boldsymbol{I}\right]\right] \tag{27}$$

The thermal expansion and freezing strain at time t_n are computed using the following expressions:

$$\boldsymbol{\varepsilon}^{th}\big(\theta(t_n)\big) = \alpha\,\big(\theta(t_n) - \theta(t_0)\big)\,\boldsymbol{I} \tag{28}$$

and

$$\boldsymbol{\varepsilon}_f\big(\theta(t_n)\big) = \varepsilon_{f0}\,\frac{1-tanh\big[m\big(\theta(t_n)-\theta_f\big)\big]}{2}\,\boldsymbol{I} \tag{29}$$

$\boldsymbol{\varepsilon}(t_n)$ can be computed from Eq. (24) when $\boldsymbol{\sigma}(t_n)$ is given. Conversely, Eq. (30) provides the stress tensor at time t_n as a function of strain and quantities related to the loading history of the material:

$$\boldsymbol{\sigma}(t_n) = 2\tilde{\mu}_n\,\boldsymbol{\varepsilon}(t_n) + \tilde{\lambda}_n\,tr\big(\boldsymbol{\varepsilon}(t_n)\big)\boldsymbol{I} + \boldsymbol{\Upsilon}_n \tag{30}$$

With

$$\boldsymbol{\Upsilon}_n = 2\tilde{\mu}_n\big[\overline{\boldsymbol{\chi}'} - \boldsymbol{\varepsilon}^{th}\big(\theta(t_n)\big) - \boldsymbol{\varepsilon}_f\,(\theta(t_n))\big] + \tilde{\lambda}_n\boldsymbol{tr}\big[\overline{\boldsymbol{\chi}'} - \boldsymbol{\varepsilon}^{\boldsymbol{th}}\big(\boldsymbol{\theta}(\boldsymbol{t_n})\big) - \boldsymbol{\varepsilon}_{\boldsymbol{f}}(\boldsymbol{\theta}(\boldsymbol{t_n}))\big]\,\boldsymbol{I} \tag{31}$$

and

$$\tilde{\lambda}_n = \frac{\nu}{(1-2\upsilon)(1+\nu)\tilde{J}_{n,n}}, \quad \text{and} \quad \tilde{\mu}_n = \frac{1}{2(1+\nu)\tilde{J}_{n,n}} \tag{32}$$

Eq (30) also reads like Hooke's law with "initial" stress $\boldsymbol{\Upsilon}_n$.

Algorithm for the computation of the mechanical response

The equations above are implemented in a numerical program. Figure 11 shows the different steps of the algorithm utilized to compute the whole set of strain and stress tensor components in response to the given ones considering variable temperature, thermal expansion and swelling strain. The developed program is used in the next section to model the behavior of dry and saturated AC during CTFS and TSRST testing.

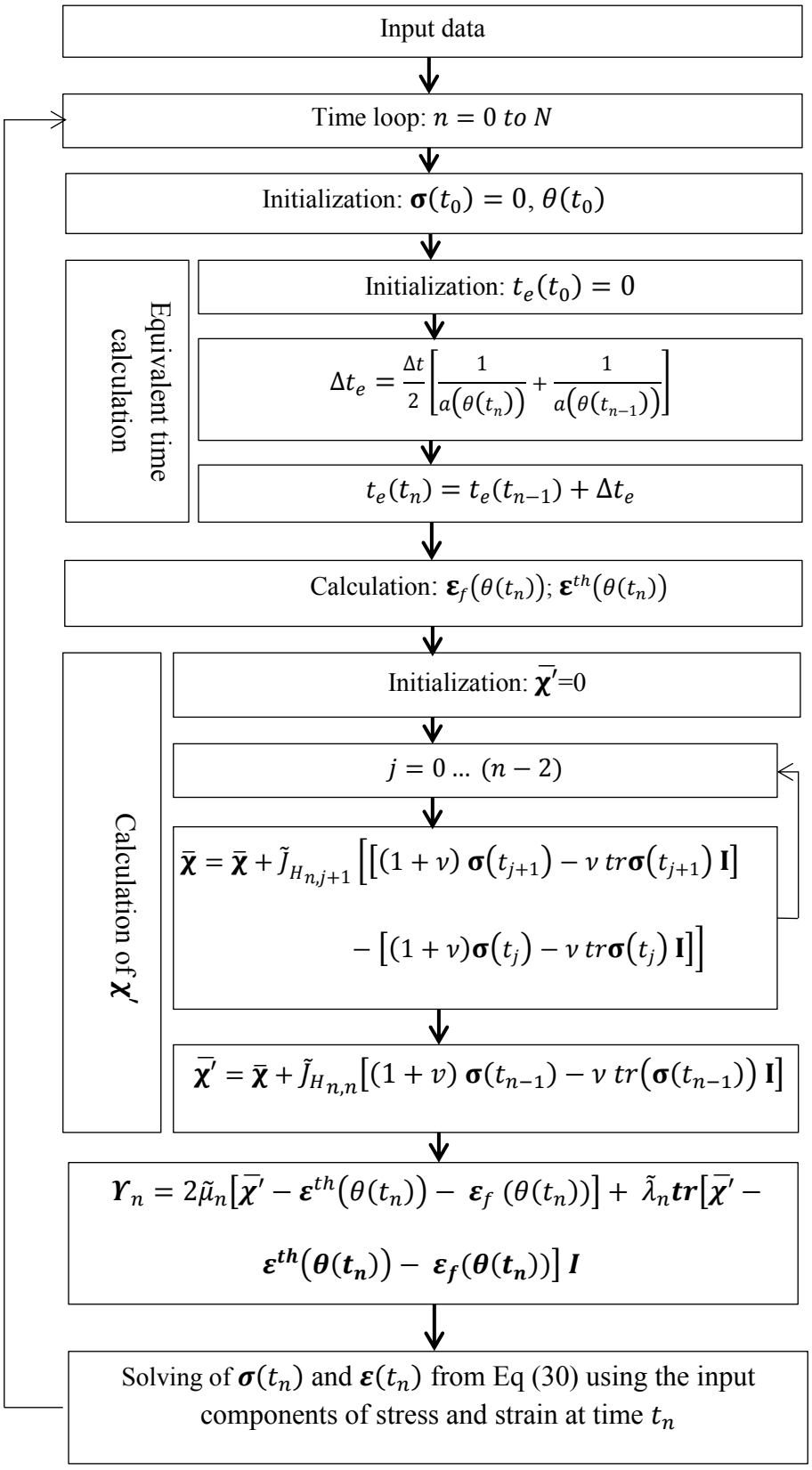

446

447 Figure 11: Algorithm for evaluation of the constitutive law under variable temperature

4. MODELING OF CTFS AND TSRST WITH THE DEVELOPED CONSTITUTIVE LAW

The developed constitutive relationship can be used now to simulate the transient response of AC samples in the CTFS and TSRST tests, assuming homogeneous temperature, strain and stress within the samples over the all duration of the tests. The numerical results are compared with the experimental data presented in section 2 obtained with the same specimen submitted to the two tests. The viscoelastic properties of the AC material are characterized from complex modulus tests [19] for the dry AC sample and the use of software Viscoanalyse to determine the Huet parameters. The values obtained are shown in Table 2. Poisson's ratio is set to 0.28. The other material parameters related to thermal expansion and freezing are inferred from the CTFS and TSRST testing (Table 2).

The input temperature for the simulations is that measured by the sensor placed at the surface of the dry specimen.

Huet model parameters	Thermal expansion coefficient $(\mu m/m/°C)$	Swelling strain coefficients
$E_\infty = 34862\ MPa$; $h = 0.57$; $k = 0.21$; $\delta = 1.96$; $\nu = 0.28$	$\alpha = 25$	$m = 5$; $\varepsilon_{f0} = 150\ \mu strain$; $\theta_f = -6\ °C$ for CTFS and $\theta_f = -10\ °C$ for TSRST

Table 2: Properties of the used AC materials

464 **CTFS test modeling**

465 In this test, stress free boundary condition applies on the outer surface of the specimen
466 $\boldsymbol{\sigma}(t) = 0$. The components of the strain tensor in cylindrical coordinates check:
467 $\varepsilon_{rr}(t) = \varepsilon_{\theta\theta}(t) = \varepsilon_{zz}(t)$ and $\varepsilon_{rz}(t) = \varepsilon_{r\theta}(t) = 0$.

468 Figure 12 shows the computed strain for the dry and saturated conditions as well as the
469 comparison with the experimental data. The model accuracy for the dry condition is
470 satisfying; a thermal expansion coefficient of $25\,\mu strain/°C$ leading to a thermal strain
471 approximately equal to $500\,\mu strain$ for $\Delta\theta = -20$ °C. On the other hand, the numerical
472 curve obtained for the saturated condition exhibits globally a similar evolution as the
473 experimental curve. However, in accordance to the modeling approach considered here only
474 one single peak is observed during the phase change time period. The model performs
475 relatively well though, when ε_{f0} is determined as the difference of strain between the plateaus
476 obtained for the dry and the saturated conditions at the end of testing.

477

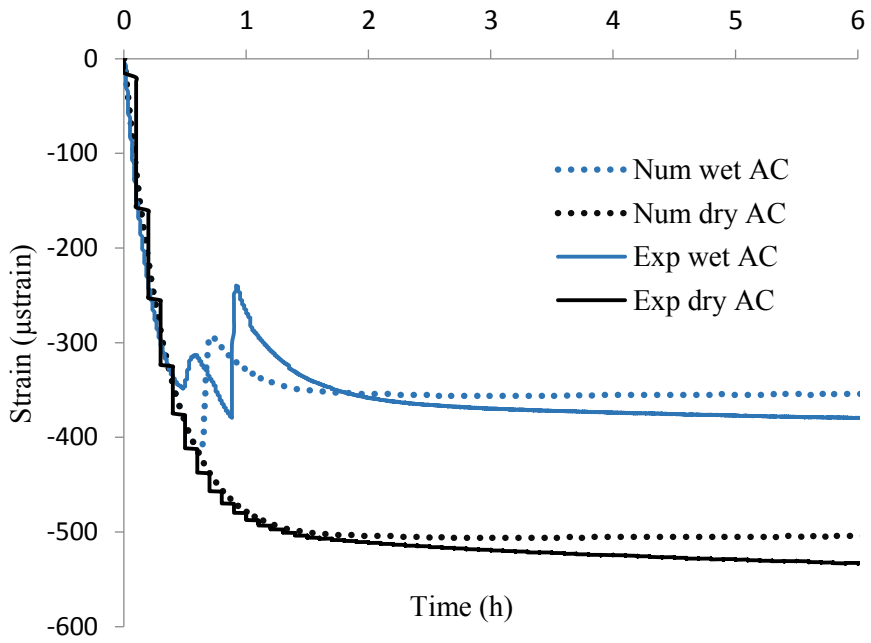

478

479 Figure 12: Comparison between the numerical results and experimental data obtained for CTFS under
480 dry and wet conditions.

481 **TSRST test modeling**

482 In that case, the two unknowns are the axial stress $\sigma_{zz}(t)$ due to the force applied by the
483 piston to ensure zero deformation of the specimen in the axial direction and the resulting
484 radial strain $\varepsilon_{rr}(t)$. The other strain and stress components are assumed zero.
485 Figure 13 shows the comparison between the curves of experimental and computed axial
486 stress obtained for dry and wet conditions. Obviously the specimen rupture observed at the
487 end of the test (Figure 6a) cannot be reproduced since not accounted for in the model. In the
488 simulations, ε_{f0} is set to zero and $150\ \mu strain$ (according to CTFS testing results) for the dry
489 and saturated conditions, respectively. As shown in Figure 13, a good agreement is obtained
490 for the dry condition revealing the relevance of the concept of equivalent time. The results
491 obtained for the saturated case are also fairly good overall. As long as temperature is greater
492 than θ_f = - 10°C, the stress evolution is superimposed with that of the dry AC. For
493 temperature around θ_f, the axial stress shows an abrupt decrease and even enter the
494 compressive domain. This phase coincides in the model with the occurrence of the peak due
495 to ε_f. This drop in the axial stress is well captured by the model as the counterpart of the
496 swelling effect modeled through ε_f. Afterwards the curve evolves similarly again to that of
497 the dry specimen but is shifted due to the drop undergone at freezing.
498

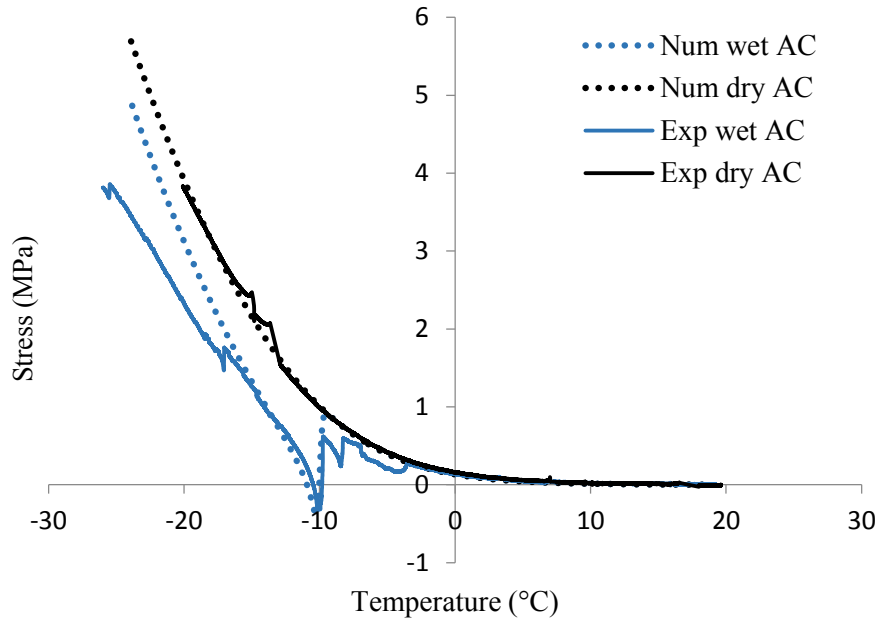

499

500 Figure 13: Comparison between TSRST experimental data and the simulated axial stress obtained for
501 the dry and partially saturated conditions

502

503 Finally, the agreement of the simulations with the experimental data is fairly good for both
504 tests what validates the developed model incorporating thermal expansion and swelling strain
505 and relying on the concept of equivalent time. It is shown that the calibration of the swelling
506 strain can be performed according to CTFS testing once full solidification of pore water has
507 taken place. Then the model makes it possible to simulate accurately the complex evolution of
508 the axial stress observed during TSRST testing of the saturated AC specimens.

509 **5. CONCLUSION**

510 The purpose of the present research was to study the thermo-mechanical behavior of partially
511 saturated asphalt concrete (AC) materials subjected to freezing. This research program was
512 initiated following the sudden damaging of asphalt pavements observed during recent winters
513 in France and Northern Europe countries.

514 Two types of experimental tests were carried out in this study; CTFS and TSRST testing were
515 performed on dry and partially saturated samples to evaluate the impact of freezing pore water
516 on the behavior of saturated AC. The test results have revealed a significant effect with
517 prominent and brutal changes of the mechanical response in terms of strain (swelling) or
518 stress of the specimens tested. In addition, these tests have indicated that deformation due to
519 thermal expansion and swelling was quite isotropic. Concerning TSRST testing, the
520 (negative) temperature at which failure occurs was found to be 12% lower for the saturated
521 specimens than for the dry ones. In that case, the critical stress at failure was also slightly
522 smaller.
523 In parallel, a tridimensional constitutive model dedicated to saturated AC materials was
524 developed on the basis of experimental results. The development of this model has taken into
525 account the following characteristics of AC: viscoelasticity, thermal expansion and swelling
526 effect under variable temperature. Discretization of this law was implemented in a numerical
527 program and was validated through simulation of the CTFS and TSRST testing.
528 It is believed that the significant frost effects observed during CTFS and TSRST transposed to
529 a pavement structure could lead to the issue mentioned above. Further steps in this research
530 will thus include testing on pavement structures and implementation of the developed
531 constitutive law in a finite element (FE) code coupling the mechanical problem to the heat
532 equation with phase change. These simulations will be used to investigate the impact of
533 swelling and self-stress effects developing at the frost front.

534 **ACKNOWLEDGMENT**

535 The authors gratefully acknowledge LHOIST Southern Europe for the financial support to
536 this work. Experimental tests in the laboratory were carried out at IFSTTAR Nantes.

REFERENCES

[1] Vulcano- GN, Kerzreho JP, Mauduit V, and Chabot A, "Stripping phenomenon of top layers of thick pavements," presented at the 11th International Conference on Asphalt Pavements, France, 2010.

[2] V. Mauduit *et al.*, "Dégradation subite des enrobés bitumineux par période de gel/dégel: Analyse de cas de terrain et recherche exploratoire en laboratoire," *Bull. Lab. Ponts Chaussées*, no. 279, p. pp–47, 2013.

[3] C. Mauduit, F. Hammoum, J.-M. Piau, V. Mauduit, S. Ludwig, and D. Hamon, "Quantifying expansion effects induced by Freeze-Thaw cycles in partially water saturated bituminous mix: Laboratory Experiments," *Road Mater. Pavement Des.*, vol. 11, no. sup1, pp. 443–457, 2010.

[4] S. Lamothe, D. Perraton, and H. Di Benedetto, "Contraction and expansion of partially saturated hot mix asphalt samples exposed to freeze–thaw cycles," *Road Mater. Pavement Des.*, vol. 16, no. 2, pp. 277–299, 2015.

[5] S.Caro, E.Masad, A.Bhasin, and D.N.Little, "Moisture susceptibility of asphalt mixtures part 1: Mechanisms," *Int. J. Pavement Eng.*, vol. 9, no. 2, pp. 81–98, Apr. 2008.

[6] S.Caro, E.Masad, A.Bhasin, and D.N.Little, "Moisture susceptibility of asphalt mixtures part 2: Characterisation and modeling," *Int. J. Pavement Eng.*, vol. 9, no. 2, pp. 99–114, 2008.

[7] R. Roberson and J. Siekmeier, "Determining material moisture characteristics for pavement drainage and mechanistic empirical design," *Res. Bull. Minn. Dep. Transp. Off. Mater. Road Res.*, 2002.

[8] X. Chen and B. Huang, "Evaluation of moisture damage in hot mix asphalt using simple performance and superpave indirect tensile tests," *Constr. Build. Mater.*, vol. 22, no. 9, pp. 1950–1962, 2008.

[9] E. Özgan and S. Serin, "Investigation of certain engineering characteristics of asphalt concrete exposed to freeze–thaw cycles," *Cold Reg. Sci. Technol.*, vol. 85, pp. 131–136, 2013.

562 [10] W. Si, B. Ma, N. Li, J. Ren, and H. Wang, “Reliability-based assessment of deteriorating
563 performance to asphalt pavement under freeze–thaw cycles in cold regions,” *Constr. Build.*
564 *Mater.*, vol. 68, pp. 572–579, 2014.
565 [11] H. Xu, W. Guo, and Y. Tan, “Permeability of asphalt mixtures exposed to freeze–thaw cycles,”
566 *Cold Reg. Sci. Technol.*, vol. 123, pp. 99–106, Mar. 2016.
567 [12] H. Xu, W. Guo, and Y. Tan, “Internal structure evolution of asphalt mixtures during freeze–thaw
568 cycles,” *Mater. Des.*, vol. 86, pp. 436–446, 2015.
569 [13] S. Lamothe, D. Perraton, and H. D. Benedetto, “Degradation of hot mix asphalt samples
570 subjected to freeze-thaw cycles and partially saturated with water or brine,” *Road Mater.*
571 *Pavement Des.*, vol. 18, no. 4, pp. 849–864, Jul. 2017.
572 [14] “NF EN 13108-1 - Mélanges bitumineux - Spécifications des matériaux - Partie 1 : enrobés
573 bitumineux.” AFNOR, 2008.
574 [15] “NF P98-250-5, Essais relatifs aux chaussées - Préparation des mélanges hydrocarbonés - Partie
575 5 : mesure en laboratoire de la masse volumique apparente d’un corps d’épreuve au banc
576 gammadensimétrique.” AFNOR, March-1993.
577 [16] C. Mauduit *et al.*, “Experimental investigation of frost/thaw effects on bituminous mixes under
578 wet conditions,” in *Asphalt Pavements*, CRC Press, 2014, pp. 139–146.
579 [17] C.Huet, “Etude par méthode d’impédance du comportement viscoélastique des matériaux
580 hydrocarbonés,” Université de Paris, 1963.
581 [18] Heck JV, “Modélisation des déformations réversibles et permanentes des enrobés bitumineux -
582 Application à l’ornièrage des chaussées,” Thèse, Université de Nantes, 2001.
583 [19] “NF EN 12697-26 - Mélanges bitumineux - Méthodes d’essai pour mélange hydrocarboné à
584 chaud - Partie 26 : module de rigidité.” AFNOR, Jun-2012.